JOURNAL OF MATERIALS SCIENCE **37** (2002) 5255–5259

The structure and thermal stability of mechanically alloyed Ni-Nb-Zr amorphous alloys

M. H. ENAYATI
Department of Materials Engineering, Isfahan University of Technology, Isfahan 84154, Iran
P. SCHUMACHER, B. CANTOR
Department of Materials, University of Oxford, Parks Road, Oxford, OX1 3PH, UK
E-mail: enquiries@materials.oxford.ac.uk

$Ni_{80}Nb_{20}$, $Ni_{60}Nb_{40}$, $Ni_{40}Nb_{60}$, $Ni_{60}Nb_{20}Zr_{20}$ and $Ni_{60}Zr_{40}$ amorphous alloys were prepared by mechanical alloying. The structure and thermal behaviour of the amorphous alloys were studied by X-ray diffractometry and differential scanning calorimetry and were compared to corresponding melt spun materials. In Ni-Nb amorphous alloys the mean nearest-neighbour distance and the thermal stability both increase with increasing Nb content. Substitution of Nb by Zr in $Ni_{60}Nb_{40}$ amorphous alloy also increases the mean nearest-neighbour distance, but reduces the thermal stability.

1. Introduction

No long range order exists in the amorphous state and the amorphous solid is characterized by only short-range atomic order. Amorphous materials exhibit remarkable properties such as mechanical, catalytic, corrosion and magnetic properties [1, 2]. This combination of physical and mechanical properties has led to commercial applications, especially in the field of magnetic materials. Amorphous alloys, whichever way they are prepared, are metastable, and on subsequent heating will lower their free energy by crystallization. Crystallization changes the properties of the amorphous alloy and, it is important therefore to control its thermal stability before using it in an application.

The aim of the present work was to study the thermal behaviour of Ni-Nb-Zr amorphous alloys prepared by mechanical alloying (MA). The results were compared with those obtained for melt-spun (MS) samples.

2. Experimental procedures

Powder mixtures of elemental Ni (<50 μm, 99.9% purity), Nb (<110 μm, 99.8% purity) and Zr (<500 μm, 99.9% purity) with compositions of $Ni_{80}Nb_{20}$, $Ni_{60}Nb_{40}$, $Ni_{40}Nb_{60}$, $Ni_{60}Nb_{20}Zr_{20}$ and $Ni_{60}Zr_{40}$ were mechanically alloyed at room temperature, using a Fritsch Pulverisette ball mill in an Ar atmosphere with a ball-to-powder weight ratio of ~10 : 1. Melt spinning was performed onto a Cu wheel rotating with a tangential speed of 50 m/s in an inert Ar atmosphere. The compositions of the samples were determined using a Cameca Su30 electron microprobe analyzer with a wavelength-dispersive X-ray spectrometer (WDX) attachment. The results are shown in Table I. For MS samples the nominal and measured compositions were close to each other indicating minimal loss of elements during ingot preparation and melt spinning. MA samples were slightly contaminated by Fe and Cr due to wear of the milling media. MA and MS samples were characterized by X-ray diffraction (XRD) in a Philips PW1729 diffractometer using filtered Cu K_α radiation ($\lambda = 0.1542$ nm), and by differential scanning calorimetry (DSC) in a TA2200 thermal analyser fitted with a 2010 DSC module using a constant heating rate of 10 K/min from 150–670°C under a dynamic Ar atmosphere. The onset temperature of each DSC peak was taken as the temperature at which the DSC signal deviated from the base-line by about 1% of the maximum peak value. The temperature at which the exotherm reached its maximum peak value was taken as the peak temperature. Samples of alloys with an end temperature of crystallization higher than or close to 670°C (the limit of the DSC) were annealed in a furnace at 760°C for 1.5 h to ensure full crystallization. Annealing was performed inside glass tubes which were evacuated to a pressure lower than 1×10^{-5} mbar and then sealed.

TABLE I Sample compositions (at.%)

Sample	Ni	Nb	Zr	Fe	Cr	Si
MA $Ni_{80}Nb_{20}$	77.78	19.40	–	2.58	0.24	–
MA $Ni_{60}Nb_{40}$	58.30	38.81	–	2.62	0.27	–
MA $Ni_{40}Nb_{60}$	38.40	58.09	–	3.14	0.35	–
MA $Ni_{60}Zr_{40}$	59.13	–	40.27	0.54	0.06	–
MA $Ni_{60}Nb_{20}Zr_{20}$	59.34	19.65	19.86	1.04	0.11	–
MS $Ni_{60}Nb_{40}$	60.10	39.85	–	–	–	0.05
MS $Ni_{60}Zr_{40}$	60.67	–	39.21	–	–	0.12
MS $Ni_{60}Nb_{20}Zr_{20}$	60.24	20.39	19.17	–	–	0.20

3. Results and discussion

3.1. Ni-Nb alloys

$Ni_{80}Nb_{20}$, $Ni_{60}Nb_{40}$ and $Ni_{40}Nb_{60}$ alloys were successfully amorphized by mechanical alloying. For all three compositions a fully amorphous structure was obtained after 85 h of milling time. The details of the structural evolution of Ni-Nb alloys during MA are given elsewhere [3]. By melt spinning, however, it was possible to produce an amorphous structure only for the $Ni_{60}Nb_{40}$ composition. Fig. 1 shows XRD traces from MA $Ni_{80}Nb_{20}$, $Ni_{60}Nb_{40}$ and $Ni_{40}Nb_{60}$ powders after 85 h mechanical alloying and from MS $Ni_{60}Nb_{40}$ ribbons. The MA and MS samples exhibited a diffuse halo characteristic of a fully amorphous structure. Fig. 2 shows the mean nearest-neighbour distance, r_1, for each of the amorphous alloys, estimated using the approximate Ehrenfest formula [4];

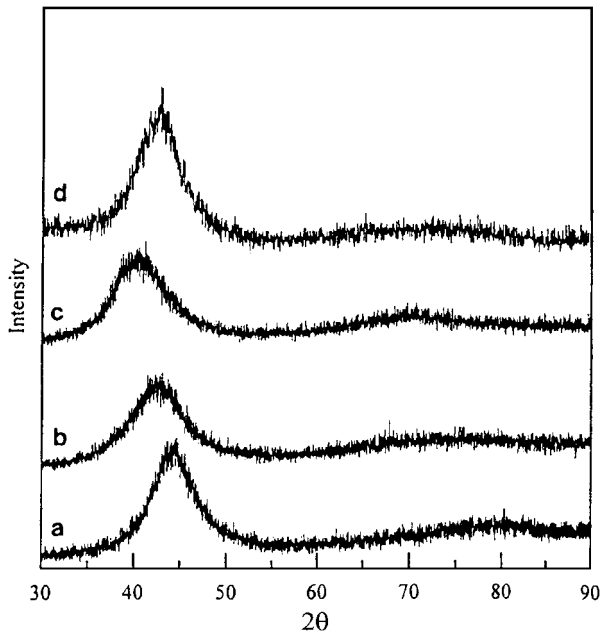

Figure 1 XRD traces from (a) MA $Ni_{80}Nb_{20}$, (b) $Ni_{60}Nb_{40}$, (c) MA $Ni_{40}Nb_{60}$ and (d) MS $Ni_{60}Nb_{40}$ amorphous alloys.

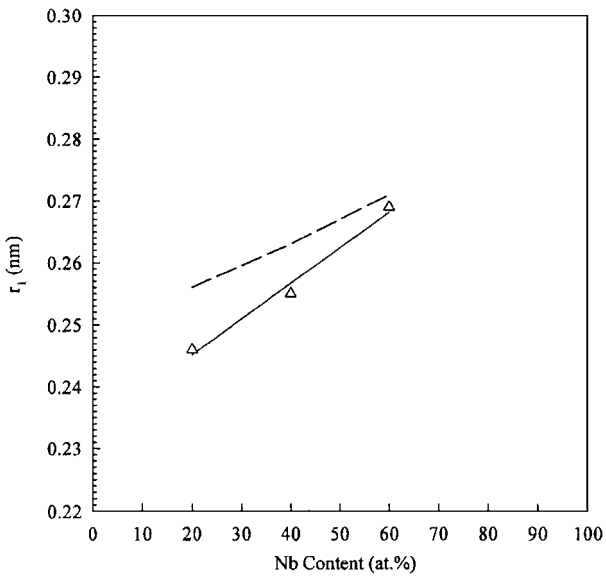

Figure 2 Mean nearest-neighbour distance r_1, for MA $Ni_{80}Nb_{20}$, $Ni_{60}Nb_{40}$ and MA $Ni_{40}Nb_{60}$ amorphous alloys. The dashed line represents the weighted r_1 values for the alloys from elemental Ni and Nb.

$$2r_1 \sin\theta_1 = 1.2\lambda \quad (1)$$

where θ_1 is the position of the amorphous halo. The amorphous halo decreased linearly to lower angles, i.e., the mean nearest-neighbour distance increased linearly with increasing Nb content. The mean nearest-neighbour distance increased from 0.246 nm for $Ni_{80}Nb_{20}$ to 0.255 nm for $Ni_{60}Nb_{40}$ and then 0.269 nm for $Ni_{40}Nb_{60}$. The r_1 value for MS $Ni_{60}Nb_{40}$ amorphous alloy was 0.254 nm in good agreement with 0.255 nm for MA $Ni_{60}Nb_{40}$. Taking interatomic distances for elemental Ni and Nb as $r_1^{Ni} = 0.249$ nm and $r_1^{Nb} = 0.285$ nm [5], the weighted r_1 value for amorphous Ni-Nb alloy follows the dashed line in Fig. 2. The weighted r_1 values especially for $Ni_{80}Nb_{20}$ and $Ni_{60}Nb_{40}$ alloys are greater than the corresponding values estimated by the Ehrenfest formula. The r_1 values are in good agreement with the previous results from the same alloys prepared by different techniques [6–8].

Fig. 3 shows DSC traces from MA $Ni_{80}Nb_{20}$, $Ni_{60}Nb_{40}$ and $Ni_{40}Nb_{60}$ amorphous alloy powders after 85 h mechanical alloying and from MS $Ni_{60}Nb_{40}$ amorphous ribbons. The $Ni_{80}Nb_{20}$ amorphous alloy exhibited two crystallization exotherms and the $Ni_{60}Nb_{40}$ and the $Ni_{40}Nb_{60}$ amorphous alloys exhibited a single crystallization exotherm over the temperature range 150–670°C. The onset and peak crystallization temperatures T_o and T_p for the MA and MS amorphous alloys are listed in Table II. The onset temperature of crystallization T_o can be taken as a criterion to compare the relative thermal stability of the three amorphous alloys. $Ni_{80}Nb_{20}$ has the lowest thermal stability against

TABLE II Onset and peak crystallization temperatures (T_o and T_p °C) and crystallization products for Ni-Nb amorphous alloys prepared by MA and MS

Sample	T_o	T_{p1}	T_{p2}	Crystallization products
MA $Ni_{80}Nb_{20}$	462	494	545	Ni_3Nb, Ni_8Nb
MA $Ni_{60}Nb_{40}$	629	662	–	Ni_3Nb, Ni_6Nb_7
MS $Ni_{60}Nb_{40}$	632	658	–	Ni_3Nb, Ni_6Nb_7
MA $Ni_{40}Nb_{60}$	630	643	–	Ni_6Nb_7

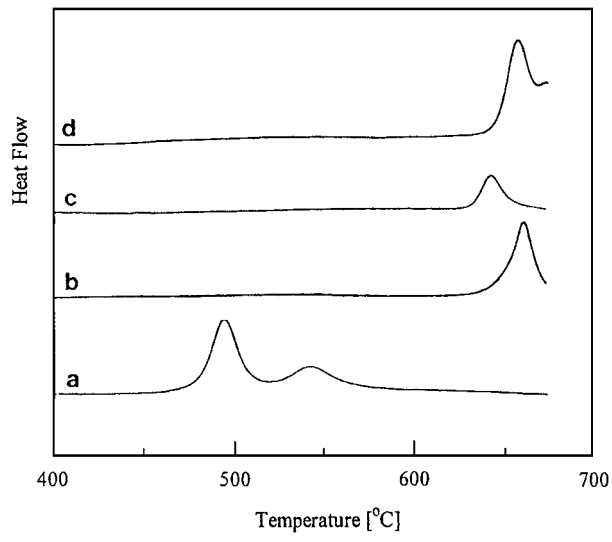

Figure 3 DSC traces from (a) MA $Ni_{80}Nb_{20}$, (b) $Ni_{60}Nb_{40}$, (c) MA $Ni_{40}Nb_{60}$ and (d) MS $Ni_{60}Nb_{40}$ amorphous alloys.

crystallization, with T_o 462°C. Increasing Nb content from 20 to 40 at.% increases T_o from 462 to 629°C. Further increasing Nb content from 40 to 60 at.% does not influence T_o significantly although the peak crystallization temperature T_p decreases. These results differ from those obtained by Barbee *et al*. [6] for Ni-Nb amorphous alloys prepared by vapour quenching. Thermal stability was determined by the first appearance of crystalline phases at high temperatures using *in situ* XRD at temperature intervals of 20°C. The crystallization temperature was found to be significantly higher at around the eutectic composition, $Ni_{60}Nb_{40}$. These results agree, however, with those obtained by Petzoldt [9] who measured the peak crystallization temperature for a series of MA Ni-Nb amorphous alloys in the composition range 20–80 at.% Ni. The peak crystallization temperature, T_p was found to vary with composition, but in the range 20–60 at.% Ni was nearly constant, at around T_p 670°C (at a heating rate of 40 K/min).

The main crystallization products for MA and MS Ni-Nb amorphous alloys after annealing at 760°C for 1.5 h are included in Table II. XRD traces after full crystallization for $Ni_{80}Nb_{20}$, $Ni_{60}Nb_{40}$ and $Ni_{40}Nb_{60}$ alloys exhibited unidentified peaks which increased in intensity with increasing Nb content. Otherwise, the final crystallization structure of $Ni_{80}Nb_{20}$ and $Ni_{60}Nb_{40}$ amorphous alloys was consistent with the expected equilibrium structure from the Ni-Nb phase diagram, containing a mixture of Ni_3Nb and Ni_8Nb for $Ni_{80}Nb_{20}$ and a mixture of Ni_3Nb and Ni_6Nb_7 for $Ni_{60}Nb_{40}$. However, the fully crystallized structure of $Ni_{40}Nb_{60}$ amorphous alloy did not contain Nb which did not agree with the phase diagram. The lack of Nb in the crystallization products of $Ni_{40}Nb_{60}$ is probably related to the formation of unknown phases.

3.2. Zr alloys

MA of $Ni_{60}Nb_{20}Zr_{20}$ and $Ni_{60}Zr_{40}$ alloys led to an amorphization reaction which was completed after 115 and 300 h milling respectively. The details of structural evolution during MA are given elsewhere [3]. $Ni_{60}Zr_{40}$ and $Ni_{60}Nb_{20}Zr_{20}$ amorphous alloys were also successfully produced by melt spinning. Figs 4 and 5 show XRD traces from MA and MS $Ni_{60}Nb_{20}Zr_{20}$ and $Ni_{60}Zr_{40}$ amorphous alloys respectively. The mean nearest neighbour distance r_1, for MA $Ni_{60}Nb_{40}$, $Ni_{60}Nb_{20}Zr_{20}$ and $Ni_{60}Zr_{40}$ amorphous alloys is plotted in Fig. 6 as a function of Zr content. The mean-nearest neighbour distance r_1 increases linearly from 0.255 nm for $Ni_{60}Nb_{40}$ to 0.259 nm for $Ni_{60}Nb_{20}Zr_{20}$ and then to 0.265 nm for $Ni_{60}Zr_{40}$ as Nb atoms are substituted with the larger Zr atoms. The mean-nearest neighbour distance r_1 for MS $Ni_{60}Nb_{20}Zr_{20}$ and $Ni_{60}Zr_{40}$ amorphous alloys were 0.260 nm and 0.264 nm respectively, in good agreement with the corresponding MA amorphous alloys.

Fig. 7 shows DSC traces from MA and MS $Ni_{60}Zr_{40}$ amorphous alloys. Both materials exhibited two crystallization exotherms at almost the same temperatures. The MA and MS alloys crystallization products were identical, a mixture of $Ni_{10}Zr_7$ and an unknown phase.

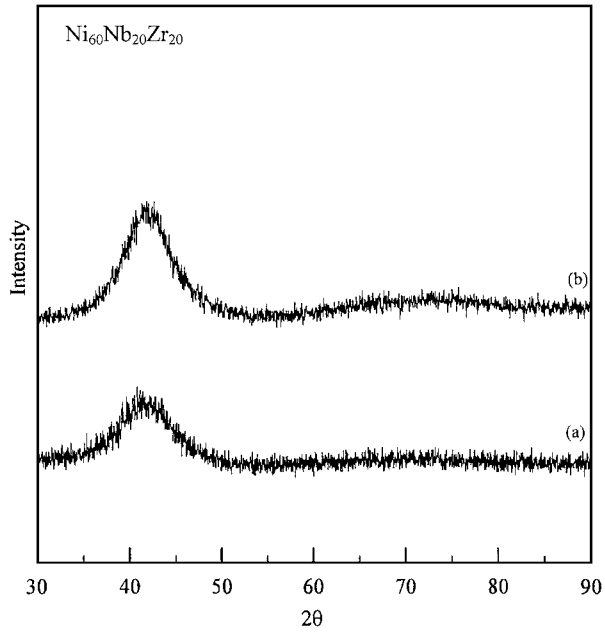

Figure 4 XRD traces from (a) MA and (b) MS $Ni_{60}Nb_{20}Zr_{20}$ amorphous alloys.

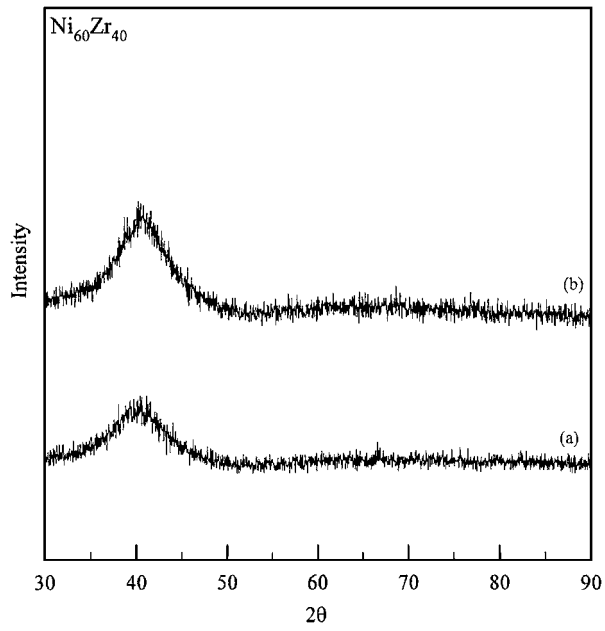

Figure 5 XRD traces from (a) MA and (b) MS $Ni_{60}Zr_{40}$ amorphous alloys.

The unknown phase could not be matched to any known compound of Zr-O, Zr-N or Ni-Zr-O.

DSC traces from MA and MS $Ni_{60}Nb_{20}Zr_{20}$ amorphous alloys are shown in Fig. 8. Both materials exhibited two overlapping crystallization exotherms at almost the same temperatures. Lack of XRD data for the ternary Ni-Nb-Zr system prevented identification of the crystallization products.

Table III lists the onset and peak crystallization temperatures of MA and MS $Ni_{60}Nb_{40}$, $Ni_{60}Nb_{20}Zr_{20}$ and $Ni_{60}Zr_{40}$ amorphous alloys. A comparison of crystallization temperatures for this alloy shows that substitution of Nb with Zr reduces the thermal stability. The decrease in thermal stability is shown by a significant decrease in onset crystallization temperature of approximate 35°C as the concentration of Zr increases by

TABLE III Onset and peak and crystallization temperatures (T_o and T_p °C) and crystallization products for $Ni_{60}(NbZr)_{40}$ amorphous alloys prepared by MA and MS

Sample	T_o	T_{p1}	T_{p2}	Crystallization products
MA $Ni_{60}Nb_{40}$	629	662	–	Ni_3Nb, Ni_6Nb_7
MS $Ni_{60}Nb_{40}$	632	658	–	Ni_3Nb, Ni_6Nb_7
MA $Ni_{60}Nb_{20}Zr_{20}$	596	–	630	–
MS $Ni_{60}Nb_{20}Zr_{20}$	593	–	623	–
MA $Ni_{60}Zr_{40}$	480	507	583	$Ni_{10}Zr_7$
MS $Ni_{60}Zr_{40}$	476	509	581	$Ni_{10}Zr_7$

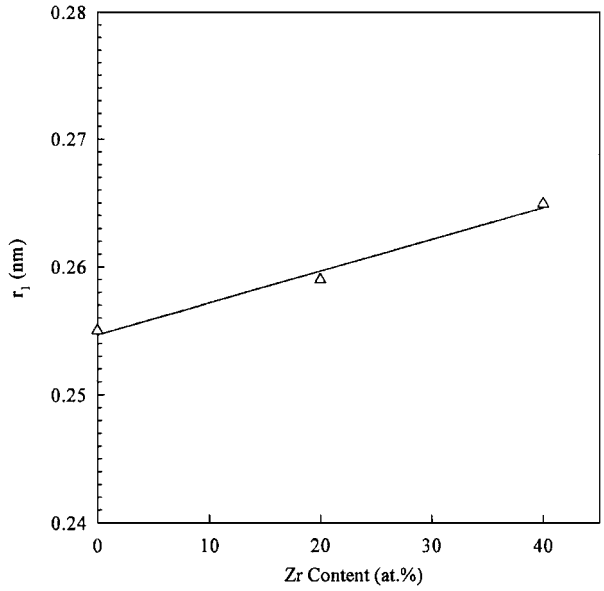

Figure 6 Mean nearest-neighbour distance r_1, for MA $Ni_{60}(NbZr)_{40}$ amorphous alloys versus Zr content.

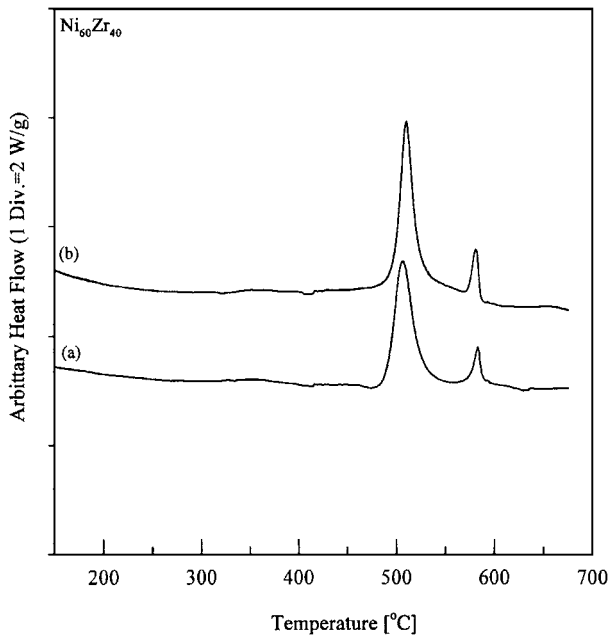

Figure 7 DSC traces from (a) MA and (b) MS $Ni_{60}Zr_{40}$ amorphous alloys.

20 at.% from $Ni_{60}Nb_{40}$ to $Ni_{60}Nb_{20}Zr_{20}$. The thermal stability decreases much more sharply, with a decrease in onset crystallization temperature of over 110°C as the concentration of Zr increases a further 20 at.% from $Ni_{60}Nb_{20}Zr_{20}$ to $Ni_{60}Zr_{40}$.

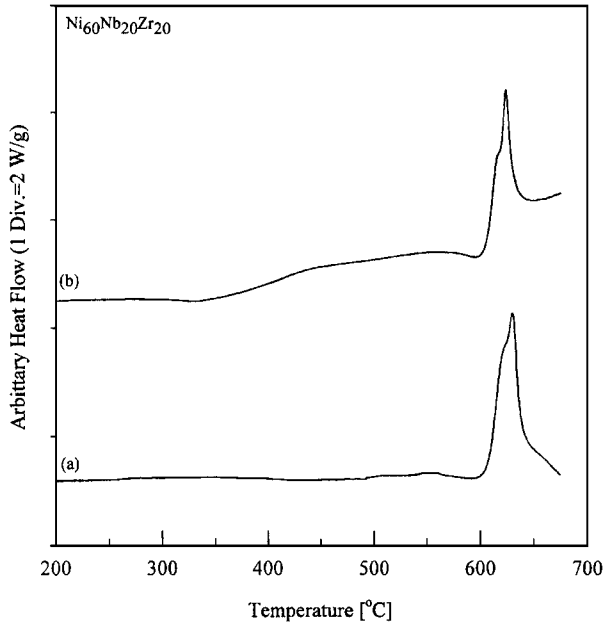

Figure 8 DSC traces from (a) MA and (b) MS $Ni_{60}Nb_{20}Zr_{20}$ amorphous alloy.

There are different previous reports about the crystallization characteristics of amorphous $Ni_{60}Zr_{40}$. Dong *et al.* [10] reported that crystallization of MS $Ni_{60}Zr_{40}$ amorphous alloy occurred in two stages. The peak crystallization temperatures were 554 and 594°C at 10°C min^{-1}. XRD traces after the first exotherm were indexed as $Ni_{10}Zr_7$, and after the second exotherm showed the presence of $Ni_{10}Zr_7$ and a second phase which could not be identified. In contrast Altounian *et al.* [11] found that the MS $Ni_{60}Zr_{40}$ amorphous alloy exhibited only one crystallization exotherm with a peak temperature of 487°C at 10°C min^{-1}. The crystallization product was $Ni_{10}Zr_7$. Haruyama and Asahi [12] as well as Eckert *et al.* [13] prepared $Ni_{60}Zr_{40}$ amorphous powders by MA and observed only one crystallization exotherm on DSC traces. The peak crystallization temperatures were reported to be 580°C (at 10°C min^{-1}) and 620°C (at 40°C min^{-1}) respectively. The discrepancies in crystallization data between the present study and those reported in the literature can be due to different levels of oxygen and nitrogen impurities introduced during sample preparation.

4. Conclusions

- Mechanical alloying can produce Ni-Nb amorphous alloy structures over a wider composition range than by melt spinning.
- In spite of basic differences in the amorphization mechanism by mechanical alloying and melt spinning, the structures as seen by XRD as well as the thermal behaviour during heat treatment are quite similar.
- In MA Ni-Nb amorphous alloys the mean nearest-neighbour distance and thermal stability both increase with increasing Nb concentration.
- Substitution of Nb by Zr in $Ni_{60}Nb_{40}$ amorphous alloy increases the mean nearest-neighbour distance, but reduces the thermal stability.

Acknowledgements

The authors would like to thank MCHE of Iran and the UK Engineering and Physical Science Research Council for financial support.

References

1. F. E. LUBORSKY, in "Encyclopedia of Materials Science and Engineering," Vol. 4, edited by M .B. Bever (Pergamon, Oxford, 1986) p. 2963.
2. H. KIMURA and T. MASUMOTO, in "Amorphous Metallic Alloys," edited by F. E. Luborsky (Butterworths, 1983) p. 187.
3. M. H. ENAYATI, D. Phil thesis, University of Oxford, 1998.
4. A. GUINIER, in "X-ray Diffraction" (Freeman, San Francisco, 1963) p. 73.
5. E. A. BRANDES and G. B. BROOK, in "Smithells Metals Reference Book" (Butterworth-Heinemann, Oxford, 1992) p. 4.
6. T. W. BARBEE, W. H. HOLMES, D. L. KEITH and M. K. PYZYNA, *Thin Solid Films* **45** (1977) 591.
7. R. C. RUHL, B. C. GIESSEN, M. COHEN and N. J. GRANT, *Acta Metall.* **15** (1967) 1693.
8. C. C. KOCH, O. B. CAVIN, C. G. McKAMEY and J. O. SCARBROUGH, *Appl. Phys. Lett.* **43** (1983) 1017.
9. F. PETZOLDT, B. SCHOLZ and H. D. KUNZE, *Mater. Sci. Eng.* **97** (1988) 25.
10. Y. D. DONG, G. GREGAN and M. G. SCOTT, *J. Non-Cryst. Solids* **43** (1981) 403.
11. Z. ALTOUNIAN, T. GUO-HUO and J. O. STROMOLSEN, *J. Appl. Phys.* **54** (1983) 3111.
12. O. HARUYAMA and Y. ASAHI, *J. Alloy Compounds* **194** (1993) 361.
13. J. ECKERT, L. SCHULTZ, E. HELLSTERN and K. URBAN, *J. Appl. Phys.* **64** (1988) 3224.

Received 5 October 2001
and accepted 27 March 2002